Structural Engineering and Mechanics, *Vol. 55, No. 4 (2015) 815-837*
DOI: http://dx.doi.org/10.12989/sem.2015.55.4.815

A family of dissipative structure-dependent integration methods

Shuenn-Yih Chang*, Tsui-Huang Wu[a] and Ngoc-Cuong Tran[a]

Department of Civil Engineering, National Taipei University of Technology, NTUT Box 2653, Taipei 106, Taiwan, Republic of China

(Received April 15, 2015, Revised July 25, 2015, Accepted July 27, 2015)

Abstract. A new family of structure-dependent integration methods is developed to enhance with desired numerical damping. This family method preserves the most important advantage of the structure-dependent integration method, which can integrate unconditional stability and explicit formulation together, and thus it is very computationally efficient. In addition, its numerical damping can be continuously controlled with a parameter. Consequently, it is best suited to solving an inertia-type problem, where the unimportant high frequency responses can be suppressed or even eliminated by the favorable numerical damping while the low frequency modes can be very accurately integrated.

Keywords: unconditional stability; explicit formulation; numerical damping; accuracy; structure-dependent integration method

1. Introduction

A series of structure-dependent integration algorithms have been successively developed by Chang (2002a, 2007, 2009, 2010, 2014, 2015) for structural dynamics. This type of integration methods is unlike the conventional step-by-step integration methods (Newmark 1959, Hilber *et al*. 1977, Wood *et al*. 1981, Chung and Hulbert 1993, Krenk 2008, Rezaiee-Pajand *et al*. 2011, Gao, *et al*. 2012, Alamatian 2013, Gui *et al*. 2014) in the formulation of the two quadrature equations, where constant coefficients are usually found for the conventional integration methods while they become functions of initial structural properties and step size for the structure-dependent integration algorithms. The most important property of the structure-dependent integration algorithms is that they can integrate the unconditional stability and explicit formulation together. Hence, a large time step can be adopted without considering stability for time integration in solving an inertia-type problem, where the total response is dominated by low frequency modes while the high frequency responses are of no interest. On the other hand, an explicit formulation implies that there is no need to involve an iteration procedure. Thus, it is computationally efficient in the time history analysis of an inertia-type problem. Notice that the choice of an appropriate step size for time integration is not only dependent upon stability and accuracy but also the capability to capture dynamic loading and linearization errors (Chen and Robinson 1993, Robinson and Chen

*Corresponding author, Professor, E-mail: changsy@ntut.edu.tw
[a]Graduate Student

http://www.techno-press.org/?journal=sem&subpage=8 ISSN: 1225-4568 (Print), 1598-6217 (Online)

1993, Chang 1998, 2001a, b, 2002b, Hadianfard 2012).

Since structure-dependent integration algorithms can have unconditional stability and explicit formulation simultaneously, it is promising if they can be further enhanced by numerical damping. This is mainly because that numerical damping can be used to suppress spurious oscillations in the numerical solution that resulted from spatially unresolved high frequency modes. It is worth noting that there are many unconditionally stable integration methods with controllable numerical damping in the currently available integration methods, such as the HHT-α method (Hilber *et al*. 1977), the WBZ-α method (Wood *et al*. 1981) and the Generalized-α method (Chung and Hulbert 1993). However, they are classified as implicit methods. This implies that their applications to nonlinear dynamic analysis will involve an iteration procedure per time step and thus more computational efforts will be consumed when compared to the explicit, structure-dependent integration methods (Chang 2002a, 2007, 2009, 2010, 2014, Kolay and Ricles 2014).

A new family of structure-dependent integration algorithms with desired numerical dissipation has been developed and is presented herein. Since the developing details are very complicated, they will not be presented although the concept will be described. However, the numerical properties of the proposed family method will be thoroughly evaluated and confirmed herein. The simultaneous integration of the unconditional stability, explicit formulation and numerical damping for this family method will be addressed in this work. In addition, the computational efficiency of this family method is also studied.

2. Dissipative integration method

Two schemes are applied to develop the new family method. One is the use of an asymptotic form of equation of motion and the other is the use of structure-dependent difference equation for displacement increment. Since the use of an asymptotic form of equation of motion to develop a dissipative integration method has been successfully implemented, such as the HHT-α method, WBZ-α method and generalized-α method, this scheme is adopted herein. Some integration methods (2002a, 2007, 2009, 2010, 2014) have been developed to integrate unconditional stability and explicit formulation together by using the structure-dependent difference equation for displacement increment and thus this scheme is also applied to develop a new family method.

As a result, the proposed dissipative integration method for a linear elastic single degree of freedom can be expressed as

$$\begin{aligned}
&\frac{2p}{p+1}ma_{i+1}+\frac{p-1}{p+1}ma_i+cv_{i+1}+kd_{i+1}=f_{i+1}\\
&d_{i+1}=d_i+\beta_1(\Delta t)v_i+\beta_2(\Delta t)^2a_i+\beta_3(\Delta t)^2a_{i-1}\\
&v_{i+1}=v_i+\frac{3p-1}{2(p+1)}(\Delta t)a_i-\frac{p-3}{2(p+1)}(\Delta t)a_{i+1}
\end{aligned} \tag{1}$$

where m, c and k are the mass, viscous damping coefficient and stiffness, respectively; d_i, v_i, a_i and f_i are the displacement, velocity, acceleration and external force at the end of the i-th time step, respectively. In general, a constant viscous damping coefficient is considered and thus $c=c_0$ is taken. Meanwhile, for a nonlinear system, k_{i+1} is used to replace k and represents the stiffness at the end of (i+1)-th time step. The coefficients β_1 to β_3 are found to be

$$\beta_1 = \frac{1}{D}\left(\frac{2}{p+1} + \frac{3-p}{p+1}\xi\Omega_0\right)$$

$$\beta_2 = \frac{1}{D}\left[\tfrac{1}{2} - \frac{p-1}{p+1} - \frac{p-1}{(p+1)^3} - \tfrac{1}{2}\left(\frac{p-1}{p+1}\right)^2 \xi\Omega_0\right] \tag{2}$$

$$\beta_3 = \frac{1}{D}\frac{p-1}{(p+1)^3}$$

$$D = \frac{2}{p+1} + \frac{3-p}{p+1}\xi\Omega_0 + \frac{1}{(p+1)^2}\Omega_0^2$$

where ξ is a viscous damping ratio; $\Omega_0 = \omega_0(\Delta t)$ and $\omega_0 = \sqrt{k_0/m}$ is the natural frequency of the system determined from the initial tangent stiffness of k_0; and p is the only parameter to control the numerical properties and $p \neq -1$, which is manifested from Eq. (1).

Based on the fundamental theory of structural dynamics, the term $\xi\Omega_0$ can be replaced with $(\Delta t)c_0/(2m)$ and the term Ω_0^2 is replaced by $(\Delta t)^2(k^0/m)$ (Chang 2002a, 2007, 2009, 2010). As a result, Eq. (2) becomes

$$\beta_1 = \frac{1}{D}\left[\frac{2}{p+1}m + \frac{3-p}{2(p+1)}(\Delta t)c_0\right]$$

$$\beta_2 = \frac{1}{D}\left[\tfrac{1}{2}m - \frac{p-1}{p+1}m - \frac{p-1}{(p+1)^3}m - \tfrac{1}{4}\left(\frac{p-1}{p+1}\right)^2 (\Delta t)c_0\right] \tag{3}$$

$$\beta_3 = \frac{1}{D}\frac{p-1}{(p+1)^3}$$

$$D = \frac{2}{p+1}m + \frac{3-p}{2(p+1)}(\Delta t)c_0 + \frac{1}{(p+1)^2}(\Delta t)^2 k_0$$

In this equation, β_1 to β_3 are functions of initial structural properties (m, c_0 and k_0) and step size (Δt). Thus, they remain invariant for a whole step-by-step integration procedure if a constant time step is used. It should be mentioned that the use of Eq. (3) to replace Eq. (2) is very important in carrying out time integration since it avoids the need to solve an eigenvalue problem, which is very time consuming for a matrix with a large order. For brevity, the Proposed Family Method will be referred as PFM subsequently.

3. Determination of parameter

Eqs. (1)-(2) reveal that the parameter p plays an important role since the equation of motion and two quadrature equations are closely related to it. Hence, it is anticipated that the numerical

properties of PFM depend upon it. Thus, it is important to determine the useful range of p so that PFM can have desired numerical properties. For this purpose, the basic analysis of PFM for a linear elastic, single degree of freedom system is needed and conducted next.

At first, the free vibration response obtained from PFM for the system can be rewritten in a recursive matrix form as

$$\mathbf{X}_{i+1} = \mathbf{A}\mathbf{X}_i \tag{4}$$

where $\mathbf{X}_{i+1}=[d_{i+1}, (\Delta t)v_{i+1}, (\Delta t)^2 a_{i+1}]^T$ and $\mathbf{A}$ is an amplification matrix. Hence, the characteristic equation of $\mathbf{A}$ can be obtained from $|\mathbf{A}-\lambda\mathbf{I}|=0$ and is found to be

$$\lambda^3 - A_1\lambda^2 + A_2\lambda - A_3 = 0 \tag{5}$$

where λ is an eigenvalue of $\mathbf{A}$ and the coefficients A_1, A_2 and A_3 are found to be

$$\begin{aligned} A_1 &= 2 - \frac{2\xi\Omega_0}{D} + \frac{1}{D}\left(\frac{p-1}{p+1}\right) - \frac{1}{D}\left[\frac{2}{(p+1)^2} + \frac{2}{p+1}\right]\Omega_0^2 \\ A_2 &= 1 - \frac{2\xi\Omega_0}{D} - \frac{2}{D}\left(\frac{p-1}{p+1}\right) - \frac{2}{D}\left[\frac{2}{(p+1)^2} - \frac{p-1}{p+1}\right]\Omega_0^2 \\ A_3 &= -\frac{1}{D}\left(\frac{p-1}{p+1}\right) \end{aligned} \tag{6}$$

Notice that this characteristic equation can be further applied to evaluate the numerical properties of PFM.

A numerical method is said to be convergent if the numerical solution approaches the exact solution as the step size tends to zero. Thus, a numerical method has to be convergent to be of any use. As a result, the parameter p must be appropriately determined so that PFM is a convergent method. A numerical method is said to be convergent if it is consistent and stable. The consistency is in terms of the order of accuracy determined from the local truncation error. Hence, the local truncation error must be derived and the stability must be evaluated for PFM.

A local truncation error is often defined as the error committed in each time step by replacing the differential equation with its corresponding difference equation (Belytschko and Hughes 1983). As a result, the local truncation error for PFM is found to be

$$\begin{aligned} E = {} & \frac{1}{D}\left[\frac{1}{p+1} - \frac{2}{(p+1)^3} - \tfrac{2}{3}\xi^2\frac{5p-7}{(p+1)^2}\right]\Omega_0^2\omega_0^2 u + \frac{1}{D}\left[\frac{2(p+2)(p-2)}{(p+1)^3} - \tfrac{4}{3}\xi^2\frac{5p-7}{(p+1)^2}\right]\xi\Omega_0^2\omega_0\dot{u} \\ & + O\left[(\Delta t)^3\right] \end{aligned} \tag{7}$$

This equation reveals that PFM can generally have a second order accuracy for any value of p and any viscous damping ratio ξ.

In the study of the stability conditions of PFM, the limiting cases of $\Omega_0 \to 0$ and $\Omega_0 \to \infty$ are considered first. Using Eq. (5), the characteristic equation of PFM and its corresponding roots for

the limiting case of $\Omega_0 \to 0$ are found to be

$$\left(\lambda + \frac{p-1}{2}\right)(\lambda - 1)^2 = 0 \quad \Rightarrow \quad \lambda_{1,2} = 1 \quad \text{and} \quad \lambda_3 = -\frac{p-1}{2} \tag{8}$$

The p value must be in the range of $-1<p\leq 3$ so that $|\lambda_3|\leq 1$ can be satisfied. Similarly, in the limit $\Omega_0 \to \infty$, the characteristic equation of PFM and its corresponding roots are found to be

$$\lambda(\lambda + p)^2 = 0 \quad \Rightarrow \quad \lambda_{1,2} = -p \quad \text{and} \quad \lambda_3 = 0 \tag{9}$$

Apparently, the stability condition of $|\lambda_{1,2}|\leq 1$ will be met if $-1<p\leq 1$ is chosen. Consequently, it is concluded that PFM can have unconditional stability in the limits $\Omega_0 \to 0$ and $\Omega_0 \to \infty$ for a linear elastic system if $-1<p\leq 1$ is met.

After obtaining the range of $-1<p\leq 1$ for PFM to have unconditional stability in the limiting cases of $\Omega_0 \to 0$ and $\Omega_0 \to \infty$, it is needed to further confirm that if the same range is applicable to a general value of Ω_0. This can be evaluated by using the Routh-Hurwitz criterion which gives necessary and sufficient conditions for the roots of polynomial to have negative real parts and using the procedure given in the reference (Lambert 1973), where $\lambda=(1+\phi)/(1-\phi)$ is used. As a result, a necessary and sufficient condition for the roots of Eq. (5) to lie within or on the circle $|\lambda|=1$ is to satisfy the following inequalities

$$\begin{aligned} &1 - A_1 + A_2 - A_3 \geq 0 \quad , \quad 3 - A_1 - A_2 + 3A_3 \geq 0 \\ &1 + A_1 + A_2 + A_3 \geq 0 \quad , \quad 3 + A_1 - A_2 - 3A_3 \geq 0 \quad , \quad 1 - A_2 + A_3(A_1 - A_3) \geq 0 \end{aligned} \tag{10}$$

After substituting Eq. (6) into Eq. (10), it is found that all the five inequalities will be met if $-1<p\leq 1$ is adopted. This proves stability for PFM. Consequently, this stability property in conjunction with the previous proof of consistency implies convergence for PFM.

4. Numerical properties

After determining the useful range of the parameter p for PFM, it is important to explore its numerical properties, such as stability, accuracy, numerical damping and overshooting. In general, these numerical properties can be obtained from Eq. (5) and the computing details can be found from the references (Belytschko and Hughes 1983, Chang 2010).

4.1 Stability

The variation of spectral radius with $\Delta t/T_0$, where $T_0=2\pi/\omega_0$, is plotted in Fig. 1 for PFM. It is very interesting to find that the spectral radius is always equal to 1 either for $p \to -1$ or $p=1$. This implies that PFM has zero numerical damping for these two cases. On the other hand, for the case of $p=0$, the spectral radius is almost equal to one for small $\Delta t/T_0$; subsequently, it decreases gradually and finally becomes a zero constant as $\Delta t/T_0$ is large enough. It is clear that the curves for $p=\pm 0.5$ are very similar to that of $p=0$ except that the constant value becomes 0.5 for a large $\Delta t/T_0$. At first glance, it seems that PFM with the p value chosen from either $-1<p\leq 0$ or $0\leq p\leq 1$ will lead to controllable numerical damping. However, it is worth noting that the curve for $p=-0.5$ shows an abrupt change of slope at the point (0.24, 0.62), which might be the bifurcation point,

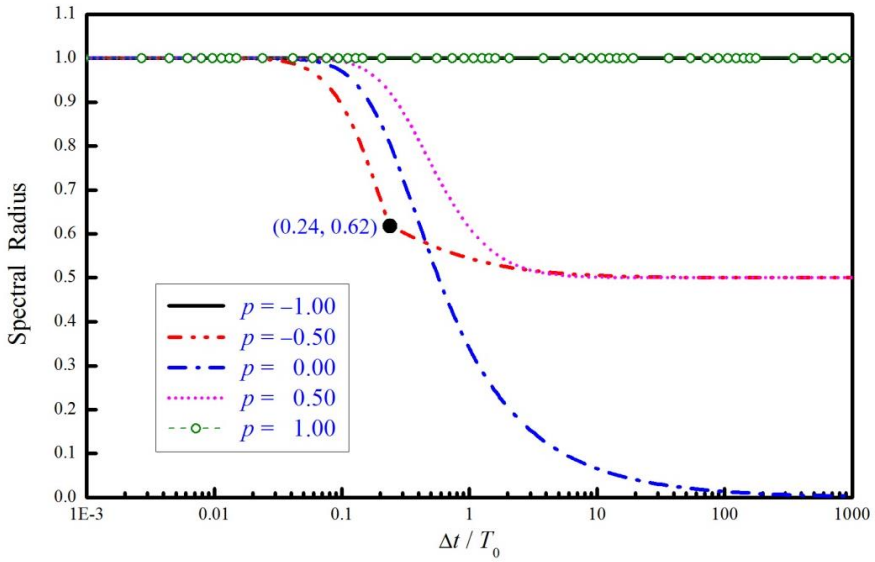

Fig. 1 Variations of spectral radius with $\Delta t/T_0$

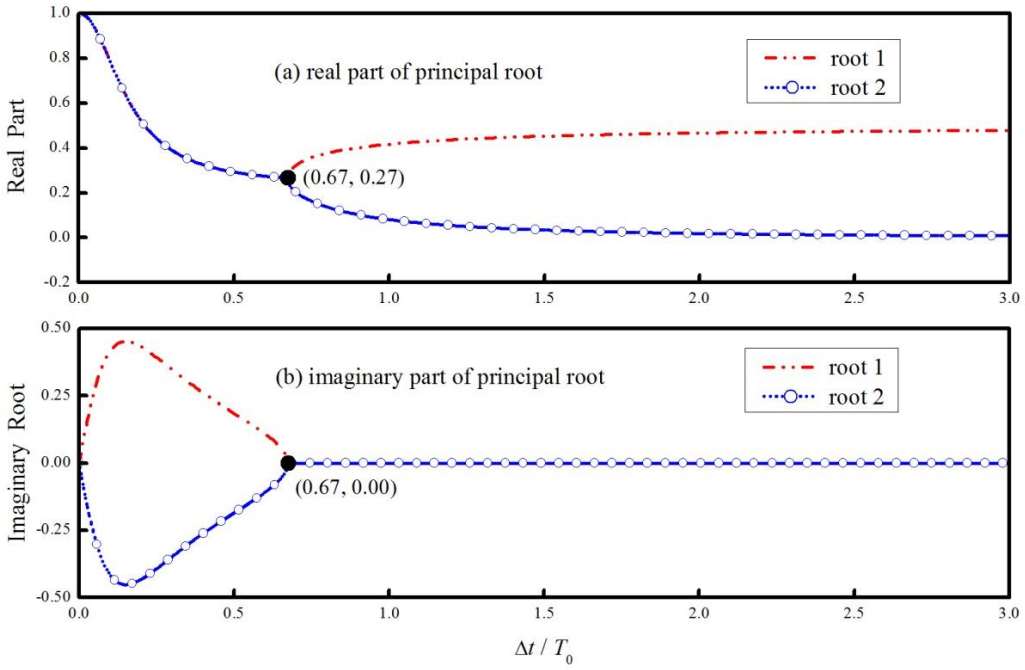

Fig. 2 Principal roots of PFM with p=−0.5

where complex conjugate roots bifurcate into real roots. Thus, it is needed to find the eigenvalues of PFM for the case of p=−0.5. For this purpose, both the real part and imaginary part of each principal root for PFM with p=−0.5 is plotted in Fig. 2. It is evident from this figure that the imaginary part of each principal root will become zero after the value of $\Delta t/T_0$ is greater than about

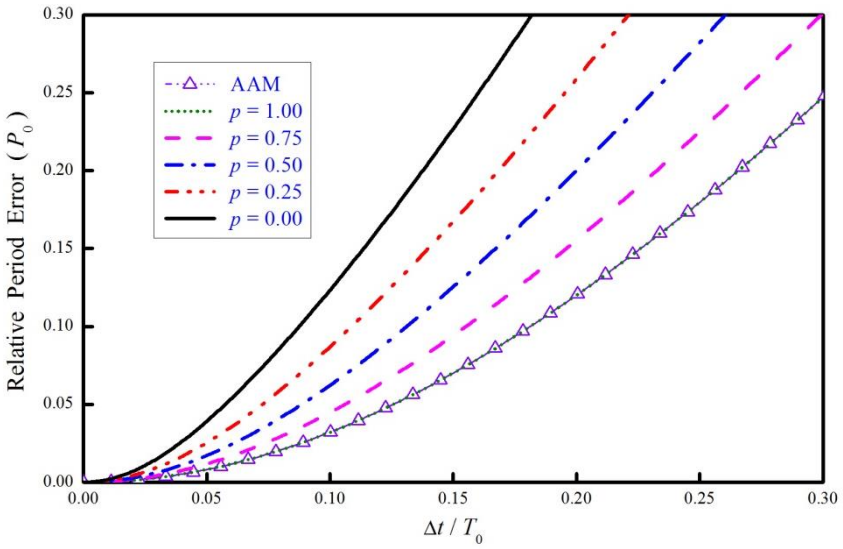

Fig. 3 Variation of relative period error with $\Delta t/T_0$

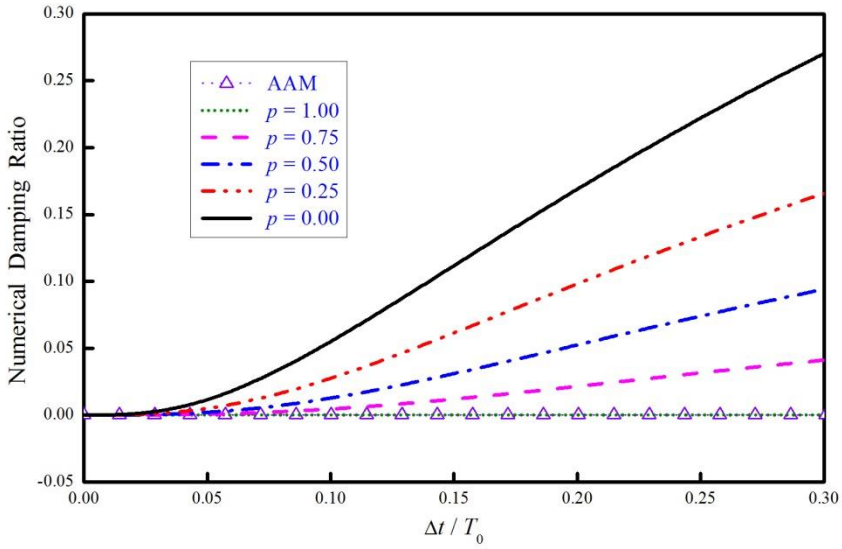

Fig. 4 Variation of numerical damping ratio with $\Delta t/T_0$

0.67, as marked in a solid circle in the figure. This confirms that the complex conjugate roots bifurcate into two real roots at this bifurcation point and thus there is no numerical damping. Hence, the range of $-1<p\leq 0$ is of no interest for practical applications. Consequently, the subsequent study will focus on the range of $0\leq p\leq 1$ for PFM.

4.2 Accuracy and numerical damping

The variations of relative period errors versus $\Delta t/T_0$ for PFM with p=1.00, 0.75, 0.50, 0.25 and

0.00 are shown in Fig. 3 while those for numerical damping ratios are plotted in Fig. 4. The corresponding results for the constant average acceleration method (AAM) are also plotted in both figures for comparisons. It is manifested from Fig. 3 that the relative period errors increase with the decrease of p for a given value of $\Delta t/T_0$. The curve for p=1.00 is overlapped with that of AAM and has the smallest relative period error for a given $\Delta t/T_0$ when compared to the other curves. In general, the relative period error is small in the range of $\Delta t/T_0 \leq 0.05$ for the five different p values. It is evident from Fig. 4 that PFM can have favorable numerical dissipation. In fact, for all the curves except for p=1.00, each curve seems to a zero damping ratio for a small value of $\Delta t/T_0$ and then increases gradually with a controlled turn upward. Finally, a constant numerical damping ratio is reached, which is manifested from Fig. 1. This implies that the low frequency modes can be accurately integrated while the high frequency modes can be effectively suppressed or even totally eliminated. Notice that the curve for PFM with p=0.00 has the largest numerical damping ratio in Fig. 4 and the largest relative period error in Fig. 3. Meanwhile, the curve for PFM with p=1.00 has no numerical damping in Fig. 4 and the smallest relative period error in Fig. 3. Hence, the increase of the numerical dissipation for PFM will sacrifice the numerical accuracy.

4.3 Overshooting

The numerical solution might overshoot the exact solution in the early response although it is calculated from an unconditionally stable integration method (Goudreau and Taylor 1972, Hilber and Hughes 1978). Therefore, the overshooting behavior for PFM must be investigated. In general, the tendency of an integration method to overshoot the exact solution can be assessed by computing the free vibration response of a single degree of freedom system for the current time step based on the previous step data. Since PFM is a convergent method, there is no overshoot as $\Omega_0 \to 0$. The behavior as $\Omega_0 \to \infty$ can provide an indication of the overshooting behavior of the high frequency mode in a system where the values of $\Delta t/T_0$ are large for the high-frequency modes. As a result, the following equations can be obtained for the limiting condition of $\Omega_0 \to \infty$.

$$\begin{aligned} d_{i+1} &\approx -p d_i \\ v_{i+1} &\approx -\frac{1}{4}(p-1)^2 \Omega_0 \omega_0 d_i + \left[\frac{1}{2}(p-1)^2 - 1\right] v_i \end{aligned} \tag{11}$$

It is manifested from this equation that there is no overshoot in displacement for any member of PFM while it has a tendency to overshoot linearly in Ω_0 in the velocity equation due to the initial displacement term except for the case of p=1.

The overshooting behavior of PFM can be revealed by computing the free vibration responses of displacement and velocity for a single degree of freedom system with a time step corresponding to $\Delta t/T_0$=10. In this calculation, the initial conditions are assumed to be d_0=1 and v_0=0. The numerical results are shown in Fig. 5. For comparison, the results obtained from AAM are also plotted in the figure. The velocity term is normalized by the initial natural frequency of the system in order to have the same unit as displacement. In Fig. 5(a), the two curves are overlapped together for AAM and PFM with p=1.0. In addition, they exhibit no overshoot both in displacement and in velocity for a linear elastic system. On the other hand, PFM with p=0.5 displays a different behavior in velocity response although it also exhibits no overshoot in displacement. In fact, a very significant overshooting phenomenon is found in velocity in the early response, as shown in Fig. 5(b). As a result, the phenomena of the overshoot behaviors either in displacement or in velocity

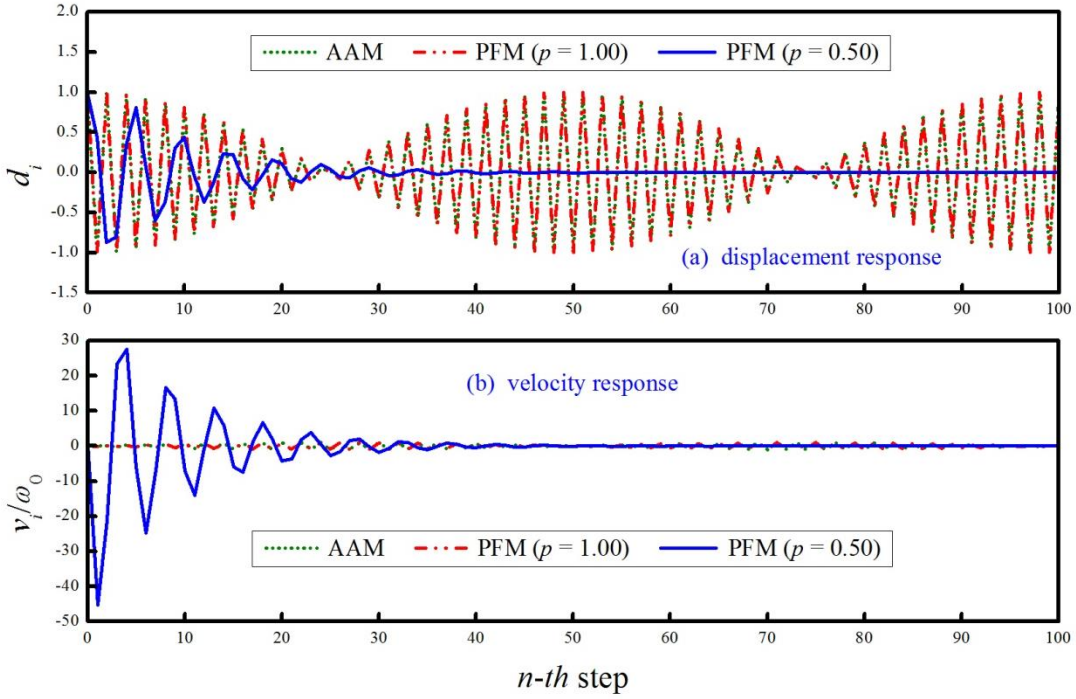

Fig. 5 Comparisons of overshoot responses for PFM

for PFM with p=1.0 and 0.5 as shown in Fig. 5 are in good agreement with the results shown in Eq. (11).

5. Implementation

After the analytical study of the numerical properties of PFM for a linear elastic system, it is important to further examine its actual performance in the solution of a nonlinear system. For this purpose, PFM is implemented for a multiple degree of freedom system. As a result, it can be expressed as

$$\begin{aligned}
&\frac{2p}{p+1}\mathbf{M}\mathbf{a}_{i+1}+\frac{p-1}{p+1}\mathbf{M}\mathbf{a}_i+\mathbf{C}_0\mathbf{v}_{i+1}+\mathbf{K}\mathbf{d}_{i+1}=\mathbf{f}_{i+1}\\
&\mathbf{d}_{i+1}=\mathbf{d}_i+\mathbf{B}_1(\Delta t)\mathbf{v}_i+\mathbf{B}_2(\Delta t)^2\mathbf{a}_i+\mathbf{B}_3\mathbf{a}_{i-1}\\
&\mathbf{v}_{i+1}=\mathbf{v}_i+\frac{3p-1}{2(p+1)}(\Delta t)\mathbf{a}_i-\frac{p-3}{2(p+1)}(\Delta t)\mathbf{a}_{i+1}
\end{aligned} \tag{12}$$

where $\mathbf{M}$, $\mathbf{C}_0$ and $\mathbf{K}$ are mass, viscous damping and stiffness matrices, respectively; $\mathbf{d}_i$, $\mathbf{v}_i$, $\mathbf{a}_i$ and $\mathbf{f}_i$ are vectors of displacement, velocity, acceleration and external force at the i-th time step, respectively. The coefficient matrices of $\mathbf{B}_1$ to $\mathbf{B}_3$ are found to be

$$\mathbf{B}_1 = \mathbf{D}^{-1}\left[\frac{2}{p+1}\mathbf{M} + \frac{3-p}{2(p+1)}(\Delta t)\mathbf{C}_0\right]$$

$$\mathbf{B}_2 = \mathbf{D}^{-1}\left[\left(\frac{1}{2} - \frac{p-1}{p+1} - \frac{p-1}{(p+1)^3}\right)\mathbf{M} - \frac{1}{4}\left(\frac{p-1}{p+1}\right)^2(\Delta t)\mathbf{C}_0\right] \tag{13}$$

$$\mathbf{B}_3 = \mathbf{D}^{-1}\frac{p-1}{(p+1)^3}\mathbf{M}$$

$$\mathbf{D} = \frac{2}{p+1}\mathbf{M} + \frac{3-p}{2(p+1)}(\Delta t)\mathbf{C}_0 + \frac{1}{(p+1)^2}(\Delta t)^2\mathbf{K}_0$$

where $\mathbf{K}_0$ is the initial stiffness matrix and the stiffness matrix $\mathbf{K}$ in the first line of Eq. (12) is generally different from the initial stiffness $\mathbf{K}_0$ for a nonlinear system. A restoring force vector $\mathbf{r}_{i+1}$ is often introduced to replace $\mathbf{K}\mathbf{d}_{i+1}$ in the solution of a nonlinear system.

The second line of Eq. (12) indicates that PFM can have an explicit formulation since it can be directly applied to determine the next step displacement vector. This is because that it only involves the previous two step data and involves no current step data. Apparently, the direct use of the coefficient matrices of $\mathbf{B}_1$ to $\mathbf{B}_3$ to determine the displacement vector $\mathbf{d}_{i+1}$ is too expensive in computing since it requires to obtain the inverse matrix of $\mathbf{D}$ and subsequently the products of matrix to matrix. Both are time consuming. Alternatively, the solution procedure of the second line of Eq. (12) is numerically equivalent to solve the equation of

$$\begin{aligned}\mathbf{D}(\mathbf{d}_{i+1} - \mathbf{d}_i) = &\left[\frac{2}{p+1}\mathbf{M} + \frac{3-p}{2(p+1)}(\Delta t)\mathbf{C}_0\right](\Delta t)\mathbf{v}_i \\ &+\left[\left(\tfrac{1}{2} - \frac{p-1}{p+1} - \frac{p-1}{(p+1)^3}\right)\mathbf{M} - \tfrac{1}{4}\left(\frac{p-1}{p+1}\right)^2(\Delta t)\mathbf{C}_0\right](\Delta t)^2\mathbf{a}_i + \frac{p-1}{(p+1)^3}\mathbf{M}(\Delta t)^2\mathbf{a}_{i-1}\end{aligned} \tag{14}$$

This equation can be solved by a direct elimination method, which consists of a triangulation and a substitution where a triangulation consumes much more computational effort than for a substitution. It is important to note that only one triangulation of $\mathbf{D}$ is needed since it is invariant for a whole integration procedure. In addition, the coefficient matrices for the velocity and acceleration terms on the right hand side of Eq. (14) are also invariant. Therefore, they can be restored for the subsequent use after the first calculations. This solution procedure for $\mathbf{d}_{i+1}$ reveals that PFM can save many computational efforts for each time step when compared to an implicit method. This is because that PFM involves no nonlinear iterations for each time step while an iteration procedure is unavoidable for an implicit method in solving a nonlinear system.

Similarly, the velocity vector can be obtained from the first and third lines of Eq. (12) and is numerically equivalent to solve the following equation

$$\begin{aligned}\left[\frac{2}{p+1}\mathbf{M} + \frac{3-p}{2(p+1)}(\Delta t)\mathbf{C}_0\right]\mathbf{v}_{i+1} = &\frac{2}{p+1}\mathbf{M}\left[\mathbf{v}_i + \frac{3p-1}{2(p+1)}(\Delta t)\mathbf{a}_i\right] \\ &+\frac{3-p}{2(p+1)}(\Delta t)\left(\mathbf{f}_{i+1} - \frac{p-1}{p+1}\mathbf{M}\mathbf{a}_i - \mathbf{r}_{i+1}\right)\end{aligned} \tag{15}$$

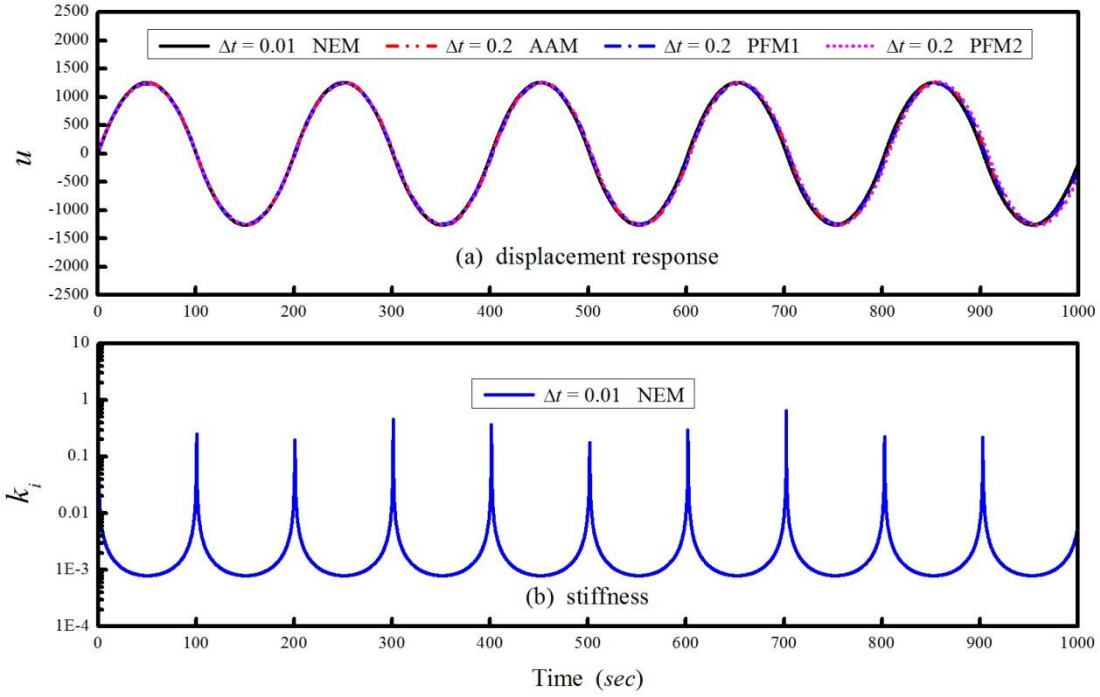

Fig. 6 Free vibration responses to mathematical nonlinearity

This equation can also be solved by a direct elimination method and only one triangulation of the matrix $2/(p+1)\mathbf{M}+(3-p)/2(p+1)(\Delta t)\mathbf{C}_0$ is needed to be performed for a whole step-by-step integration procedure. In addition, there is also no matrix-matrix product on the right hand side of Eq. (15). Apparently, no nonlinear iterations are involved for calculating the velocity vector. Finally, the acceleration vector can be calculated by using the equations of motion, i.e., the first line of Eq. (12). The implementation details of PFM reveal that it can have an explicit formulation and involves no nonlinear iterations in the solution of a nonlinear system. Hence, it is anticipated that it is computationally efficient when compared to an implicit method in solving an inertia-type problem. An explicit formulation may not be yielded for the proposed family method when internal force and velocity are nonlinearly depended.

6. Numerical illustrations

Analytical studies of PFM reveal that it has very promising numerical properties for a linear elastic system. Therefore, it is of interest to confirm the obtained analytical results for linear elastic systems and to examine its performance in the solution of nonlinear systems. In addition, the study of computational efficiency is also of great interest since PFM integrates the explicit formulation and unconditional stability together. In this numerical study, PFM with p=0.1 and 0.5 will be intensively used in the following numerical demonstrations since the former method possesses no numerical damping while the latter method shows controllable numerical damping. For brevity, the former method will be referred as PFM1 and the latter method is PFM2.

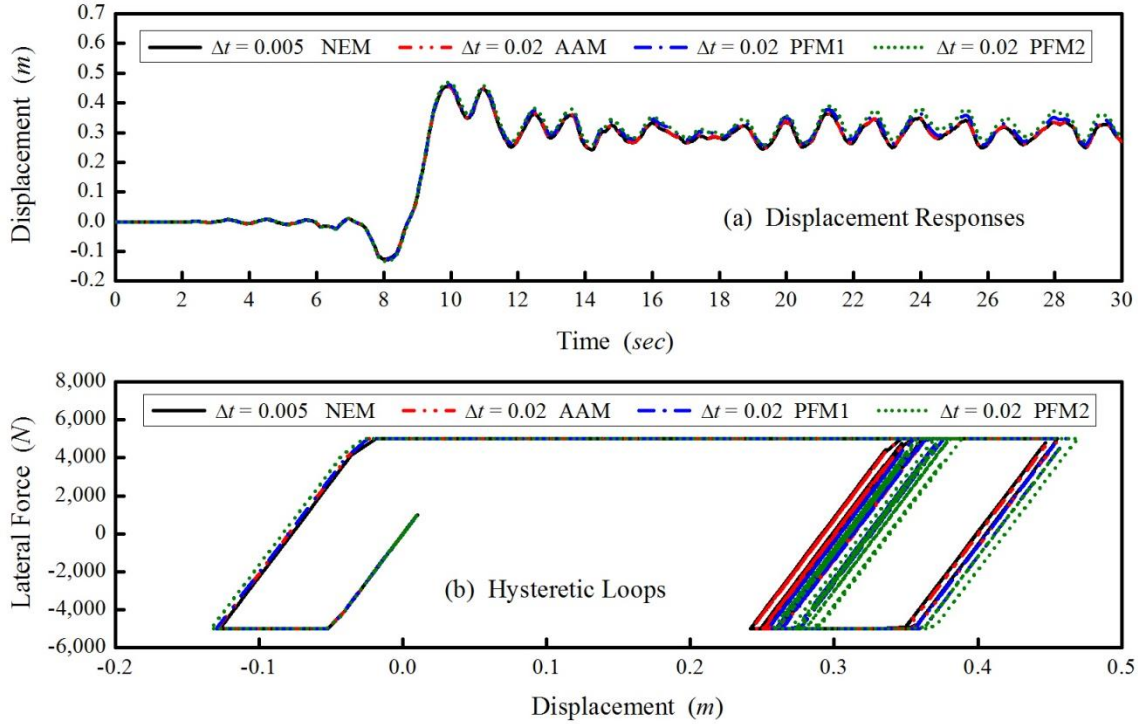

Fig. 7 Seismic responses to elastoplastic nonlinearity for one-story building

6.1 Example 1-Response to mathematical nonlinearity

A second-order differential equation is mathematically designated and it can be considered as the equation of motion for a single degree of freedom system with varied stiffness. In fact, it is

$$\ddot{u} + \frac{u}{1+|u|} = 0 \tag{16}$$

where the case of stiffness softening will be encountered for nonzero displacement. In addition, the degree of stiffness softening will increase for a large value of u. The initial period of the system is found to be 2π sec for u=0. The free vibration responses to the initial conditions of $u(0)$=0 and $\dot{u}(0)$=50 are calculated by the Newmark explicit method (NEM), AAM, PFM1 and PFM2.

Fig. 6 shows the calculation results. The solution obtained from NEM with Δt=0.01 sec can be considered as a reference solution for comparison. It is manifested from Fig. 6(a) that AAM, PFM1 and PFM2 with a time step of Δt=0.2 sec can result in a reliable solution. This time step is in correspondence to $\Delta t/T_0$=0.032≤0.05. In order to look into the variation of stiffness during the free vibration, the time history of stiffness is plotted in Fig. 6(b). It is evident that the system is experienced highly nonlinear stiffness softening since the stiffness k_i roughly varies in the range of $10^{-3}<k_i\leq 1$. This example indicates that both PFM1 and PFM2 can be applied to solve a highly nonlinear system and lead to the numerical solution with comparable accuracy when compared to the result obtained from AAM.

6.2 Example 2-Seismic response to elastoplastic nonlinearity

A one-story building with an elastoplastic model is considered in this example. The lumped mass of 4×10^3 kg and the stiffness of 10^5 N/m are assumed for the building. This building has an initial natural frequency of $5\,\text{rad/sec}$ based on the initial structural properties. On the other hand, the yielding strength of the elastoplastic model is assumed to be 5×10^3 N for both compression and tension. The ground acceleration record of TCU075 with a peak ground acceleration of 0.8 g is inputted into the building. TCU075 was collected from the main shock of 1999 Chi-Chi earthquake in Taiwan. This record is a near-field ground motion data and has a significant pulse-like wave in the velocity wave form (Loh *et al*. 2000).

Since the interval of digitization of TCU075 is $0.005\,\text{sec}$, the numerical result obtained from NEM with Δt=0.005 sec is considered as a reference solution for comparison purposes. On the other hand, the time step of Δt=0.02 sec are used to carry out time integration for AAM, PFM1 and PFM2. Apparently, this time step of Δt=0.02 will lead to almost no period distortion since the value of $\Delta t/T_0$=0.016 is much smaller than 0.05. Hence, the key factor to have a reliable solution is to minimize the linearization errors of the elastoplastic model. The numerical results for displacement response and hysteretic loop are plotted in Fig. 7. It is evident from Fig. 7(a) that AAM, PFM1 and PFM2 can have acceptable solutions although slight errors are visible in the late response time histories. That the yielding point is not exactly captured might be responsible for the slight errors. The very complicated elastoplastic behavior of the one-story building is revealed by Fig. 7(b). Thus, it is confirmed that PFM1 and PFM2 can be employed to solve a highly nonlinear problem with an elastoplastic model.

6.3 Example 3-Response to 7-story building

In order to illustrate the effectiveness of using high-frequency numerical damping to filter out the spurious participation of high frequency modes for PFM, a 7-story shear-beam type building is considered. The building is shown in Fig. 8, where a lumped mass is assumed for each story and the stiffness of each story consists a linear part and a nonlinear part. The linear part is a constant stiffness and the nonlinear part is a function of the story drift. The stiffness for each story can be expressed in the form of

$$k_{j-i} = k_{0-i}\left(1 + p_i\sqrt{|\Delta u_i|}\right) \quad , \quad \Delta u_i = u_i - u_{i-1} \quad , \quad i = 1 \sim 7 \tag{17}$$

where $k_{j\text{-}i}$ is the instantaneous stiffness for the i-th story at the end of the j-th time step and $k_{0\text{-}i}$ is the initial stiffness for the i-th story at the start of the motion; Δu_i is the story drift for the i-th story and p_i is a given constant corresponding to this story drift. The initial natural frequencies and the 1st and 7th modal shapes of the building are also shown in Fig. 8. Two initial conditions are intentionally designated to confirm the effectiveness of numerical damping for PFM. The 1st initial displacement condition only contains the pure 1st mode, i.e., $\mathbf{u}_1(0)=\phi_1/10$. Whereas, the 2nd initial displacement condition consists of the 1st and 7th modes with an equal weight, i.e., $\mathbf{u}_2(0)=\phi_1/10+\phi_7/10$. Meanwhile, two different stiffness properties are specified so that a linear elastic system and a nonlinear system can be simulated. The p_i values for the two systems are given as below:

(A) $p_1 \sim p_7 = 0.0$ a linear elastic system

(B) $p_1 \sim p_7 = -0.5$ a nonlinear system

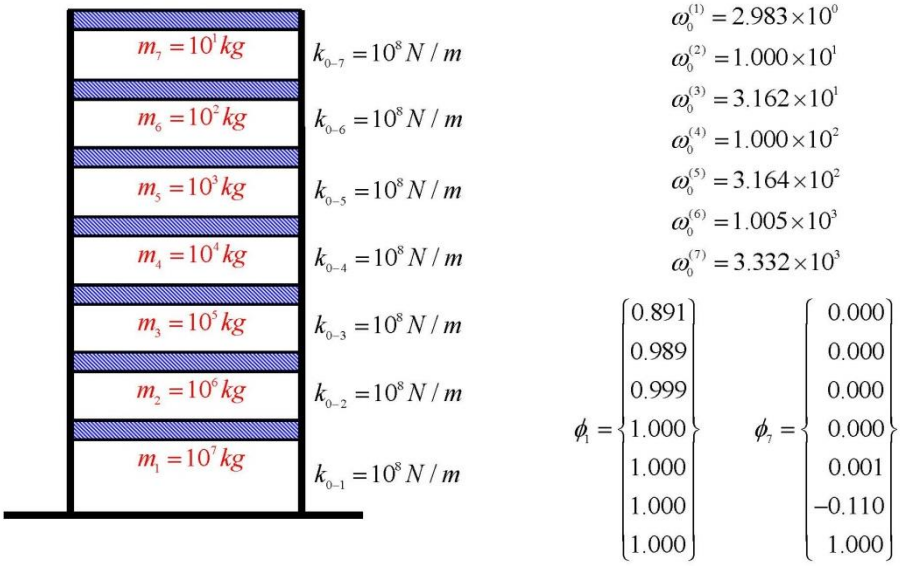

Fig. 8 A 7-story building and its structural properties

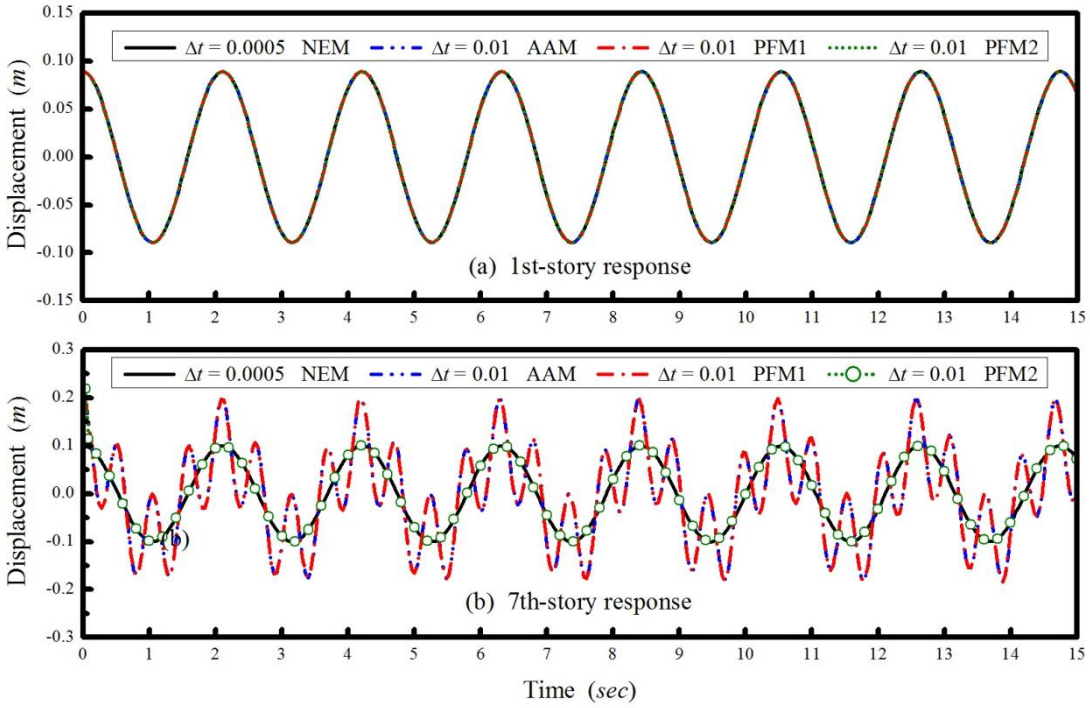

Fig. 9 Free vibration responses of linear elastic 7-story building

The free vibration response to $\mathbf{u}_1(0)$ is obtained from NEM with a time step of Δt=0.0005 sec, which is small enough to satisfy the upper stability limit $\omega_0^{(7)}(\Delta t) = 1.67 \le 2.0$. Meanwhile, the

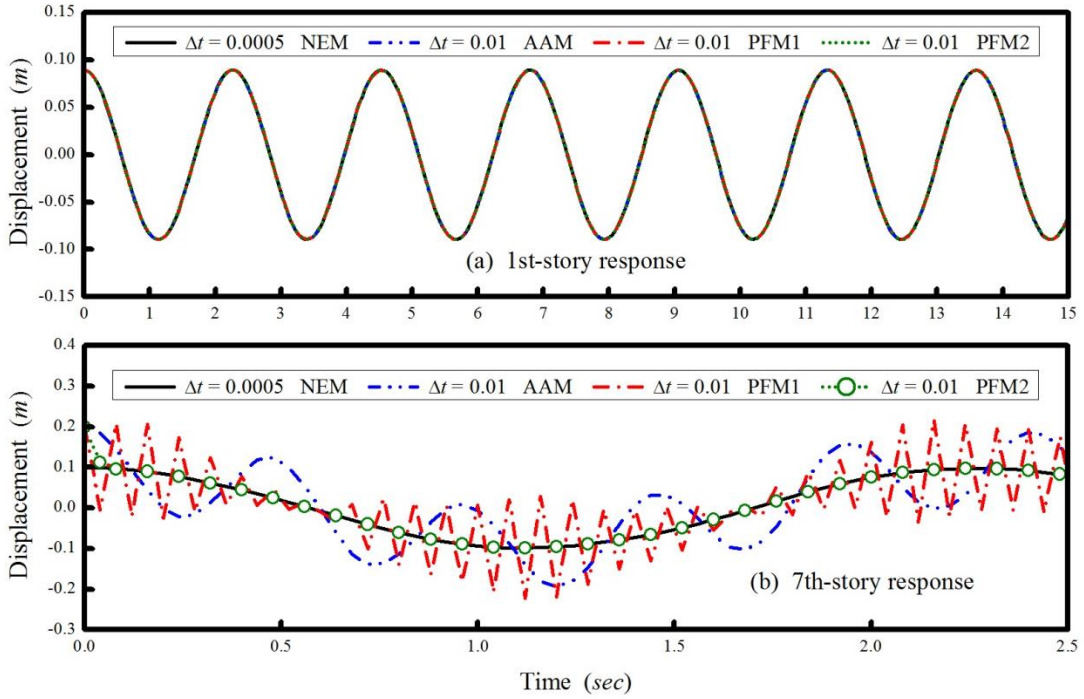

Fig. 10 Free vibration responses of nonlinear 7-story building

free vibration responses to $\mathbf{u}_2(0)$ are computed by using AAM, PFM1 and PFM2 with a time step of Δt=0.01 sec.

The displacement responses of the 1st and 7th stories for the linear elastic system are shown in Fig. 9 while those for the nonlinear system are plotted in Fig. 10. The solution obtained from NEM can be considered as an exact solution for comparison purpose since it only contains the pure 1st modal response. In Fig. 9(a), the four curves are overlapped together. This implies that AAM, PFM1 and PFM2 can give very accurate solutions for the 1st story. This is because that there is almost no contribution from the 7th mode to the total response at the 1st story and the time step of Δt=0.01 sec is small enough to accurately integrate the 1st modal response. On the other hand, in Fig. 9(b), the numerical results obtained from AAM and PFM1 drastically deviate from the exact solution while the result obtained from PFM2 is also almost coincided with the reference solution except for the very early response. This is because that AAM and PFM1 possess no numerical damping to filter out the 7th modal response while PFM2 has controllable numerical dissipation to remove the 7th modal response and thus it leads to a very reliable solution. Very similar phenomena are found in Fig. 10 for the nonlinear system. Notice that only part of the displacement responses for the 7th story are plotted in Fig. 10(b) in order to have a closer examination of using numerical damping to eliminate the 7th modal response.

6.4 Example 4-Confirmation of convergence rate for PFM without dynamic loading

It is manifested from Eq. (7) that PFM is a second-order accurate method based on the evaluation of local truncation error. This analytical prediction can be further verified by numerical

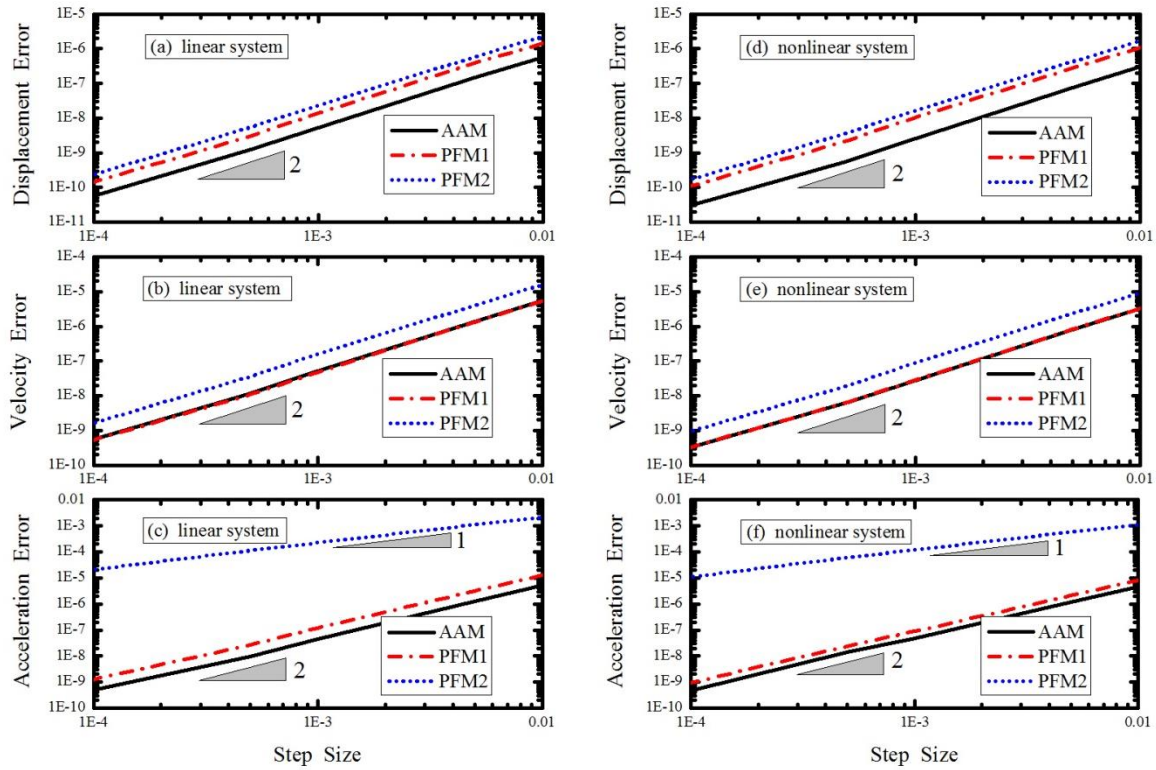

Fig. 11 Convergence of displacement, velocity and acceleration without dynamic loading

study. In fact, Example 3 can be applied to examine the convergence rate of PFM by calculating the displacement, velocity and acceleration. This can be done by next. At first, a series of different time steps, which must be small enough to yield accurate solutions, are employed to compute the free vibration responses to $\mathbf{u}_2(0)$ by using AAM, PFM1 and PFM2. In addition, the displacement error of $|d_i - u(t_i)|$, velocity error of $|v_i - \dot{u}(t_i)|$ and acceleration error of $|a_i - \ddot{u}(t_i)|$ at the instant time of t=0.1 sec are also calculated. Notice that $u(t_i)$, $\dot{u}(t_i)$ and $\ddot{u}(t_i)$ are introduced to denote the exact displacement, velocity and acceleration at the instant time of t=0.1 sec and are obtained from a very small time step. As a result, the log of the error versus the log of step size on log-log scale is plotted in Fig. 11.

In Fig. 11, it is found that that the slopes of the displacement errors and the velocity errors evaluated at the instant time of t=0.1 sec for PFM1 and PFM2 are almost the same as those of AAM and show a convergence rate of 2 for both the linear elastic and nonlinear systems. Although a similar phenomenon is also found for the acceleration error at the instant time of t=0.1 sec for AAM and PFM1 and a convergence rate of 2 is also found for the two systems, the results for PFM2 are different from those obtained from AAM and PFM1 and only show a convergence rate about 1 for the two systems.

6.5 Example 5-Confirmation of convergence rate for PFM with dynamic loading

The convergence rate of PFM was confirmed in the previous example through the calculation

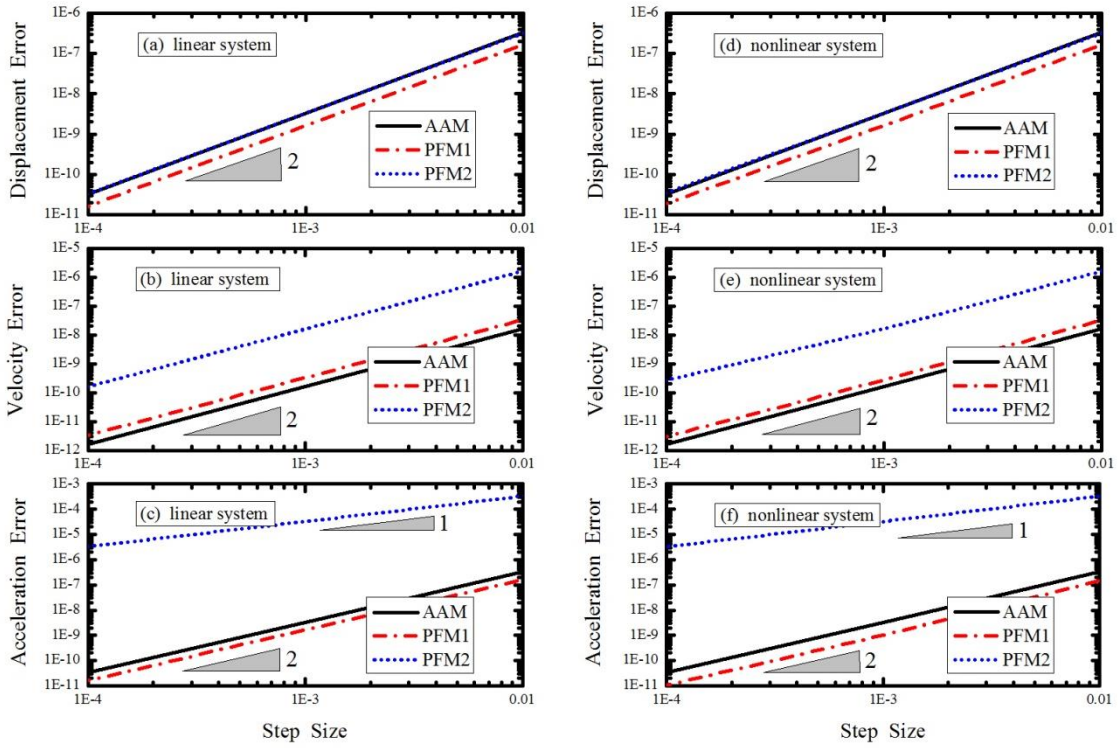

Fig. 12 Convergence of displacement, velocity and acceleration with dynamic loading

of the free vibration responses of the 7-story building. These results cannot reflect the convergence rate of PFM under dynamic loading. Hence, it is of interest to investigate its convergence rate under dynamic loading. For this purpose, a single degree of freedom system subject to the dynamic load of sin(t/10) N is considered. In fact, the following two systems are solved.

$$\begin{aligned} &\ddot{u}+u=\sin\left(t/10\right) && \text{linear elastic system} \\ &\ddot{u}+\frac{u}{1+|u|}=\sin\left(t/10\right) && \text{nonlinear system} \end{aligned} \tag{18}$$

Similar to the plot of Fig. 11, the log of the error versus the log of step size on log-log scale is plotted in Fig. 12, where the time instant of t=0.2 sec is considered.

Apparently, the phenomena found in Fig. 11 are also found in Fig. 12. In fact, the slopes of the displacement errors and the velocity errors at the instant time of t=0.2 sec for PFM1 and PFM2 seem to be the same as those of AAM and have a convergence rate of 2 for both the linear elastic and nonlinear systems. On the other hand, although the slopes of the acceleration errors at the instant time of t=0.2 sec for AAM and PFM1 also show a convergence rate of 2 for the two systems, a smaller convergence rate about 1 is found for PFM2 for both systems. As a result, it is illustrated that PFM can have a second order accuracy for the case of nonzero dynamic loading.

6.6 Example 6-Computational efficiency

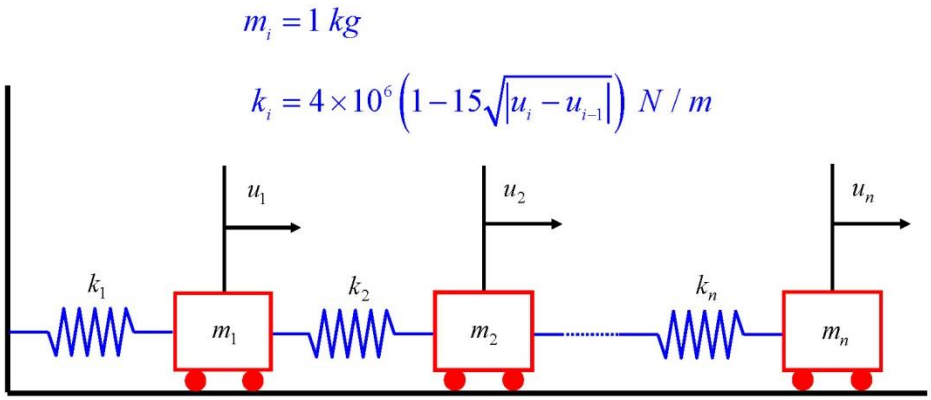

Fig. 13 A *n*-degree-of-freedom spring-mass system

Table 1 The lowest and highest initial natural frequencies

n	$\omega_0^{(1)}$ rad/sec	$\omega_0^{(n)}$ rad/sec
250	12.54	4000.00
500	6.28	4000.00
1000	3.14	4000.00

Since PFM can integrate explicit formulation and unconditional stability together, it might be very computational efficiency in solving an inertia-type problem. In order to thoroughly confirm the computational efficiency of PFM, a large spring-mass system is designated for this purpose. The system is shown in Fig. 13, where the stiffness k_i of each spring will decrease after the system deforms due to the nonlinear term of $-6\times10^7\sqrt{|u_i-u_{i-1}|}$. A 250-degree-of-freedom (250-DOF) system can be simulated if n is taken to be 250. Similarly, a 500-DOF system and a 1000-DOF system are simulated by choosing n=500 and 1000, respectively. For comparisons, NEM, AAM, Chang explicit method (CEM) (Chang 2002a, 2007), HHT–α method with α=−1/3 (HHT) (Hilber *et al*. 1977), Optimal U0-V0 algorithm with ρ_∞=1/2 (TAM) (Zhou and Tamma 2006) and PFM2 are used to calculate the displacement responses. The three spring-mass systems are excited by a sinusoidal load of $A\sin(t)$ at their base, where the amplitude A is taken to be 10, 5 and 1 in correspondence to 250-DOF, 500-DOF and 1000-DOF systems. The lowest and highest initial natural frequencies of the three systems are summarized in Table 1 for brevity.

It is seen in Table 1 that the three systems have the same highest initial natural frequency and is as large as 4000.0 rad/sec. This implies that a time step less than or equal to $\Delta t=5\times10^{-4}$ sec is needed for using NEM to solve any of the three systems. Hence, $\Delta t=5\times10^{-4}$ sec is adopted for solving the three systems. Since this time step is much smaller than accuracy consideration, it will lead to a very reliable solution and can be considered as an exact solution for comparison. On the other hand, there is no limitation on step size to meet an upper stability limit for the rest integration methods since they are unconditionally stable. In fact, the maximum allowable time step to yield an accurate result for the 250-DOF system is 0.025 sec for the rest integration methods. Whereas, those for the 500-DOF and 1000-DOF systems are 0.05 and 0.04 sec, correspondingly.

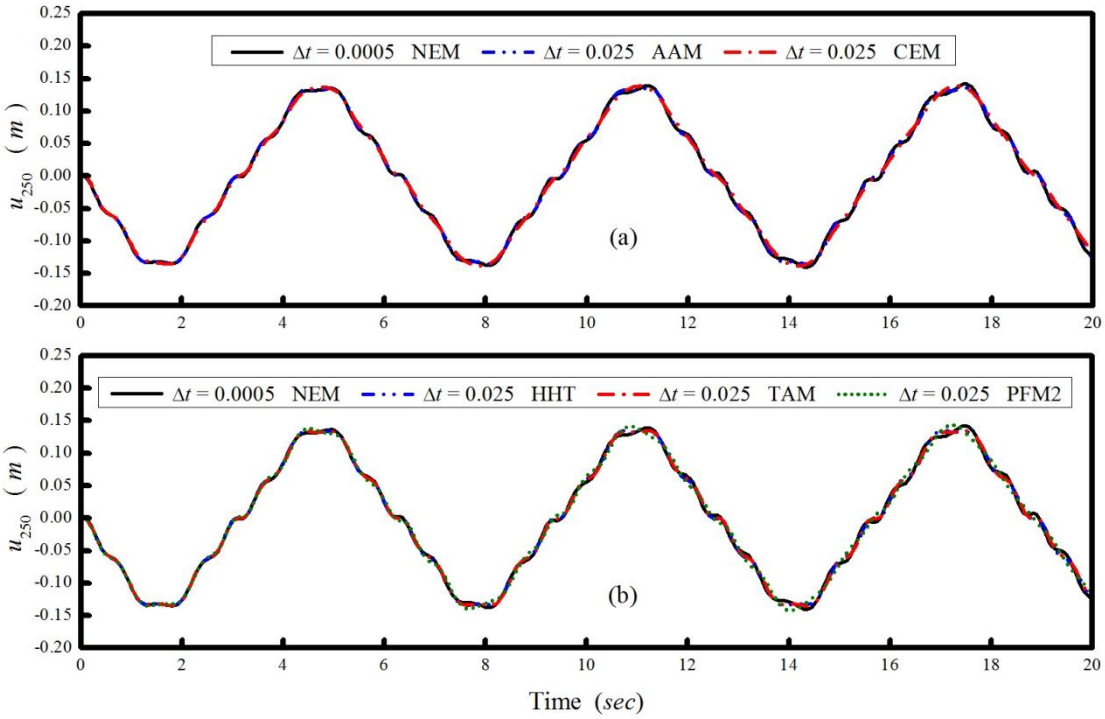

Fig. 14 Forced vibration responses of 250-DOF system

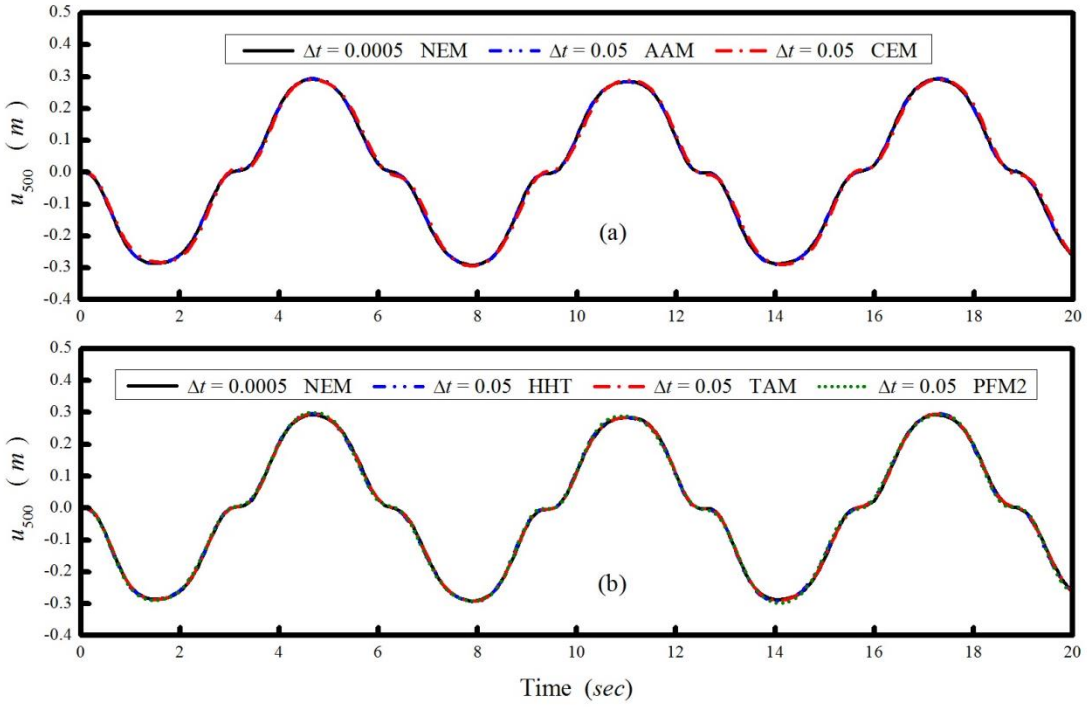

Fig. 15 Forced vibration responses of 500-DOF system

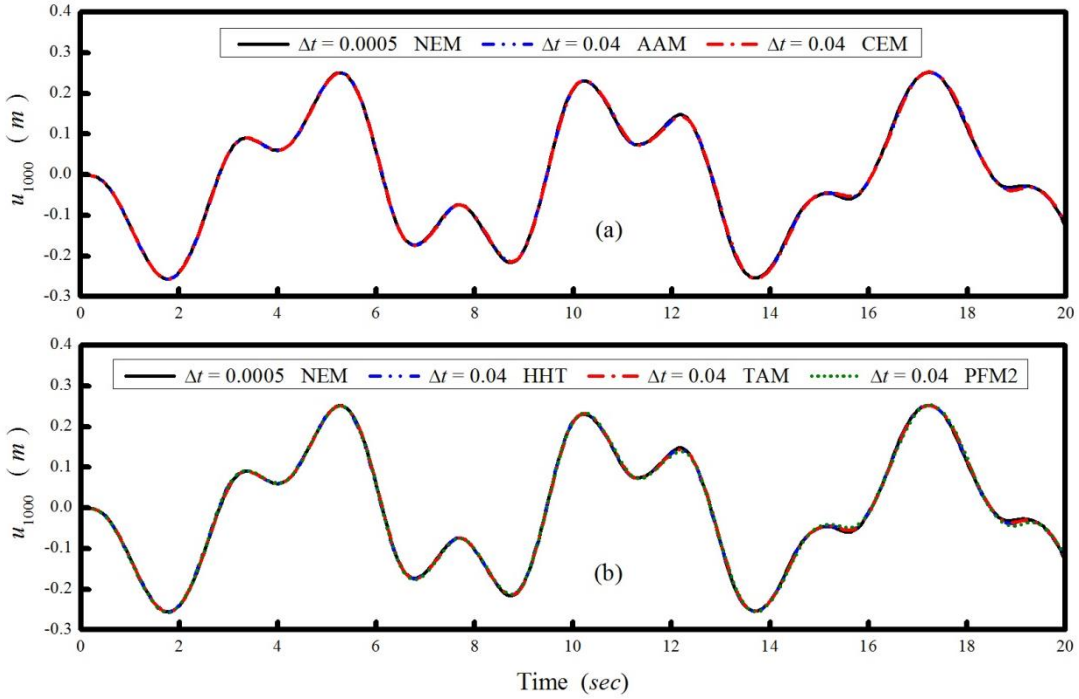

Fig. 16 Forced vibration responses of 1000-DOF system

Numerical results for the 250-DOF system are shown in Fig. 14 while those for the 500-DOF and 1000-DOF systems are plotted in Figs. 15 and 16, respectively. The top plot of each figure shows the numerical results obtained from NEM, AAM and CEM while those obtained from NEM, HHT, TAM and PFM2 are plotted in the bottom plot of each figure. It is worth noting that HHT, TAM and PFM2 can have desired numerical dissipation while NEM, AAM and CEM possess no numerical damping. An iteration procedure is needed for using AAM, HHT, and TAM since they are implicit methods. In each computation, the Newton-type iteration method is adopted to conduct the time integration procedure. It is seen in the two plots of Fig. 14 that the use of Δt=0.025 sec is able to obtain reliable solutions for the 250-DOF system for using AAM, CEM, HHT, TAM and PFM2. Therefore, it is strongly indicated that PFM2 is unconditionally stable since the product of the initial highest natural frequency and step size is as large as 100. Besides, it is also confirmed that PFM2 can have comparable accuracy when compared to AAM, CEM, HHT and TAM. Very similar phenomena are also found for the 500-DOF and 1000-DOF systems as shown in Figs. 15 and 16, respectively.

To evaluate the computational efficiency of PFM2 in contrast to NEM, AAM, CEM, HHT and TAM, the CPU time consumed for each time history analysis is recorded and summarized in Table 2. In addition, the average iteration number per time step is also shown in a parenthesis right behind the consumed CPU time for AAM, HHT and TAM. The ratio of the CPU time consumed by PFM2 over that of AAM is listed in the 9th column while that for TAM is shown in the last column. The 8th column reveals that PFM2 involves much less CPU time when compared to NEM, AAM, HHT and TAM. The use of a small time step to meet the upper stability limit is responsible for involving large CPU time for NEM. Notice that it is computationally inefficient for using NEM

Table 2 Comparison of CPU time

N-DOF	Δt	NEM	AAM	CEM	HHT	TAM	PFM2	PFM2/AAM	PFM2/TAM
250	0.025	38	205(3.7)	1.2	206(3.7)	326(6.6)	1.3	0.63%	0.40%
500	0.05	215	1303(6.2)	3.7	1350(6.4)	1745(8.5)	4.1	0.31%	0.23%
1000	0.04	1068	8543(2.4)	15.8	8953(2.4)	11342(4.0)	20.9	0.24%	0.18%

to solve an inertia-type problem such as the three systems. However, it is applied to emphasize the importance of using an unconditionally stable integration method to solve such problems. On the other hand, although the unconditional stability of AAM, HHT and TAM enables the use of a large time step to perform the time integration procedure, many computational efforts are still consumed as shown in the 4^{th}, 6^{th} and 7^{th} columns. This is because that an iteration procedure is needed in each time step for an implicit method and it is very time consuming for a matrix of large order. The integration of explicit formulation and unconditional stability together results in r saving many computational efforts for PFM2. In fact, the unconditional stability allows it use a large time step and the explicit formulation allows it involve no nonlinear iteration for each time step. The last two columns reveal that the CPU time consumed by PFM2 is less than 1% of that consumed by AAM and TAM for all the cases. In addition, it seems that the ratio will become small as the total number of degree of freedom increases. It is manifested from the 5^{th} column that the CPU time involved by CEM is slightly less than that of PFM2. This is because that it also integrates unconditional stability and explicit formulation together. In addition, its implementation is slightly simpler than for PFM2. However, it has no numerical dissipation.

7. Conclusions

Since numerical damping can be used to effectively filter out the spurious oscillations of high frequency responses, it is beneficial for an integration algorithm to have such a numerical damping property. For this purpose, a family of dissipative integration methods is proposed and presented in this work. A unique parameter p is introduced to control the numerical properties of this family method. In general, it has unconditional stability, second order accuracy and favorable numerical dissipation, which can be continuously controlled by the parameter p. In addition, it exhibits no overshooting in displacement while a tendency to overshoot in velocity is found due to the initial displacement term. Since the proposed family method can integrate unconditional stability and explicit formulation together, it is anticipated that it can save many computational efforts when compared to the use of an implicit method to solve an inertia-type problem. This is mainly because that it involves no nonlinear iterations for each time step. It is evident from numerical experiment that the CPU time consumed by the proposed family method might be as less as about 0.24% of that consumed by the constant average acceleration method in solving an inertia-type problem for a 1000-degree-of-freedom system.

Acknowledgments

The author is grateful to acknowledge that this study is financially supported by the National Science Council, Taiwan, R.O.C., under Grant No. NSC-100-2221-E-027-062.

References

Alamatian, J. (2013), "New implicit higher order time integration for dynamic analysis", *Struct. Eng. Mech.*, **48**(5), 711-736.

Belytschko, T. and Hughes, T.J.R. (1983), *Computational Methods for Transient Analysis*, Elsevier Science Publishers B.V., North-Holland.

Chang, S.Y., Tsai, K.C. and Chen, K.C. (1998), "Improved time integration for pseudodynamic tests", *Earthq. Eng. Struct. Dyn.*, **27**, 711-730.

Chang, S.Y. (2001a), "Application of the momentum equations of motion to pseudodynamic testing", *Phil. Tran. Royal Soc.*, Series A, **359**(1786), 1801-1827.

Chang, S.Y. (2001b), "Analytical study of the superiority of the momentum equations of motion for impulsive loads", *Comput. Struct.*, 79(15), 1377-1394.

Chang, S.Y. (2002a), "Explicit pseudodynamic algorithm with unconditional stability", *J. Eng. Mech.*, ASCE, **128**(9), 935-947.

Chang, S.Y. (2002b), "Integrated equations of motion for direct integration methods", *Struct. Eng. Mech.*, **13**(5), 569-589.

Chang, S.Y. (2007), "Improved explicit method for structural dynamics", *J. Eng. Mech.*, ASCE, **133**(7), 748-760.

Chang, S.Y. (2009), "An explicit method with improved stability property", *Int. J. Numer. Meth. Eng.*, **77**(8), 1100-1120.

Chang, S.Y. (2010), "A new family of explicit method for linear structural dynamics", *Comput. Struct.*, **88**(11-12), 755-772.

Chang, S.Y. (2014), "A family of non-iterative integration methods with desired numerical dissipation", *Int. J. Numer. Meth. Eng.*, **100**(1), 62-86.

Chang, S.Y. (2015), "Dissipative, non-iterative integration algorithms with unconditional stability for mildly nonlinear structural dynamics", *Nonlin. Dyn.*, **79**(2), 1625-1649.

Chen, C. and Robinson, A. (1993), "Improved time-history analysis for structural dynamics. I: treatment of rapid variation of excitation and material nonlinearity", *J. Eng. Mech.*, ASCE, **119**(12), 2496-2513.

Chung, J. and Hulbert, G.M. (1993), "A time integration algorithm for structural dynamics with improved numerical dissipation: the generalized-α method", *J. Appl. Mech.*, **60**(6), 371-375.

Gao, Q., Wu, F., Zhang, H.W., Zhong, W.X., Howson W.P. and Williams, F.W. (2012), "A fast precise integration method for structural dynamics problems", *Struct. Eng. Mech.*, **43**(1), 1-13.

Goudreau, G.L. and Taylor, R.L. (1972), "Evaluation of numerical integration methods in elasto- dynamics", *Comput. Meth. Appl. Mech. Eng.*, **2**, 69-97.

Gui, Y., Wang, J.T., Jin, F., Chen, C. and Zhou, M.X. (2014), "Development of a family of explicit algorithms for structural dynamics with unconditional stability", *Nonlin. Dyn.*, **77**, 1157-1170.

Hadianfard, M.A. (2012), "Using integrated displacement method to time-history analysis of steel frames with nonlinear flexible connections", *Struct. Eng. Mech.*, **41**(5), 675-689.

Hilber, H.M., Hughes, T.J.R. and Taylor, R.L. (1977), "Improved numerical dissipation for time integration algorithms in structural dynamics", *Earthq. Eng. Struct. Dyn.*, **5**, 283-292.

Hilber, H.M. and Hughes, T.J.R. (1978), "Collocation, dissipation, and 'overshoot' for time integration schemes in structural dynamics", *Earthq. Eng. Struct. Dyn.*, **6**, 99-118.

Kolay, C. and Ricles, J.M. (2014), "Development of a family of unconditionally stable explicit direct integration algorithms with controllable numerical energy dissipation", *Earthq. Eng. Struct. Dyn.*, **43**, 1361-1380.

Krenk, S. (2008), "Extended state-space time integration with high-frequency energy dissipation", *Int. J. Numer. Meth. Eng.*, **73**, 1767-1787.

Lambert, J.D. (1973), *Computational Methods in Ordinary Differential Equations*, John Wiley, London.

Loh, C.H., Lee, Z.K., Wu, T.C. and Peng, S.Y. (2000), "Ground motion characteristics of the Chi-Chi earthquake of 21 September 1999", *Earthq. Eng. Struct. Dyn.*, **29**, 867-897.

Newmark, N.M. (1959), "A method of computation for structural dynamics", *J. Eng. Mech. Div.*, ASCE, **85**, 67-94.

Robinson, A. and Chen, C. (1993), "Improved time-history analysis for structural dynamics. II: reduction of effective number of degrees of freedom", *J. Eng. Mech.*, ASCE, **119**(12), 2514-2530.

Rezaiee-Pajand, M., Sarafrazi, S.R. and Hashemian, M. (2011), "Improving stability domains of the implicit higher order accuracy method", *Int. J. Numer. Meth. Eng.*, **88**, 880-896.

Rezaiee-Pajand, M. and Sarafrazi, S.R. (2010), "A mixed and multi-step higher-order implicit time integration family", *J. Mech. Eng. Sci.*, **224**, 2097-2108.

Wood, W.L., Bossak, M. and Zienkiewicz, O.C. (1981), "An alpha modification of Newmark's method", *Int. J. Numer. Meth. Eng.*, **15**, 1562-1566.

Zhou, X. and Tamma, K.K. (2006), "Algorithms by design with illustrations to solid and structural mechanics/dynamics", *Int. J. Numer. Meth. Eng.*, **66**, 1738-1790.

PL